

pubs.acs.org/ac Article

Effects of Experimental Conditions on the Signaling Fidelity of Impedance-Based Nucleic Acid Sensors

Vasileia Vogiazi, Armah de la Cruz, William R. Heineman, Ryan J. White,* and Dionysios D. Dionysiou*



Cite This: Anal. Chem. 2021, 93, 812-819



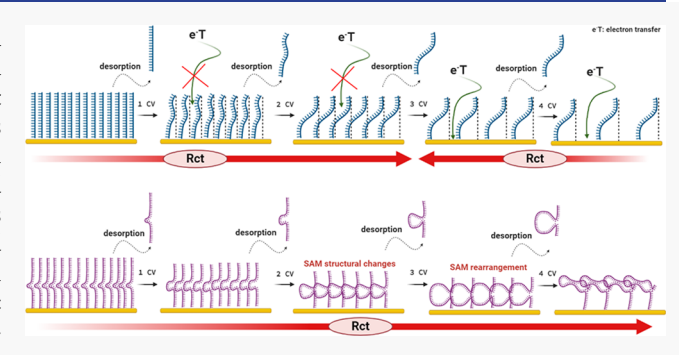
ACCESS

III Metrics & More

Article Recommendations

Supporting Information

ABSTRACT: Electrochemical impedance spectroscopy (EIS), an extremely sensitive analytical technique, is a widely used signal transduction method for the electrochemical detection of target analytes in a broad range of applications. The use of nucleic acids (aptamers) for sequence-specific or molecular detection in electrochemical biosensor development has been extensive, and the field continues to grow. Although nucleic acid-based sensors using EIS offer exceptional sensitivity, signal fidelity is often linked to the physical and chemical properties of the electrode—solution interface. Little emphasis has been placed on the stability of nucleic acid self-assembled monolayers (SAMs) over repeated voltammetric and impedimetric analyses. We have studied the stability



and performance of electrochemical biosensors with mixed SAMs of varying length thiolated nucleic acids and short mercapto alcohols on gold surfaces under repeated electrochemical interrogation. This systematic study demonstrates that signal fidelity is linked to the stability of the SAM layer and nucleic acid structure and the packing density of the nucleic acid on the surface. A decrease in packing density and structural changes of nucleic acids significantly influence the signal change observed with EIS after routine voltammetric analysis. The goal of this article is to improve our understanding of the effect of multiple factors on EIS signal response and to optimize the experimental conditions for development of sensitive and reproducible sensors. Our data demonstrate a need for rigorous control experiments to ensure that the measured change in impedance is unequivocally a result of a specific interaction between the target analyte and nucleic recognition element.

INTRODUCTION

Electrochemical sensors employing nucleic acids as biorecognition elements have become ubiquitous because of the specificity, sensitivity, quick response, low cost, and portability they provide compared to conventional methods, such as enzyme-linked immunosorbent assays, bioassays, and chromatographic methods. 1-3 The sensor surfaces typically require nucleic acids to be immobilized on an electrode. In addition, typically, these surfaces comprise self-assembled monolayers (SAMs) of nucleic acids on gold surfaces mixed with a short hydroxyl-terminated alkylthiol diluent such as mercaptohexanol (MCH).^{5,6} The formation of the sensing SAMs includes sequential steps of various thiol modifications (e.g., thiolated DNA and MCH⁶) followed by electrochemical investigation of the modified surface after each step. This is a common approach for the fabrication and characterization of sensing monolayers.^{5–8} SAMs on gold are relatively facile to form and control and are known to produce relatively stable and reproducible sensing interfaces. Nucleic acid-based sensing surfaces have been utilized extensively for hybridization detection or for small-molecule or protein detection, when using nucleic acid aptamers.⁷⁻⁹ Nucleic acid assays enable label-free detection approaches that can be applied for medical and environmental use. 10-12

Electrochemical impedance spectroscopy (EIS) is a powerful technique providing exceptional sensitivity when coupled with nucleic acid-based sensors. 13,14 EIS utilizes an AC excitation voltage to interrogate the electrode-solution interface and provides detailed information about the charge-transfer resistance and capacitance of the interface—both of which are affected by the presence of nucleic acids or any other molecules interacting with the surface. The AC frequency is varied over a wide range (from 1 MHz to 10 kHz), and electrical response to this AC excitation signal is recorded. Typically, the real parts of impedance (resistance) are plotted against the imaginary part (reactance) to yield a Nyquist plot (Figure S1). Because EIS provides information about the interfacial properties of an electrode surface, 14 it is sensitive not only to structural changes in the nucleic acid itself but also to changes in the underlying SAM that supports the sensing

Received: August 2, 2020 Accepted: December 16, 2020 Published: January 4, 2021





surface.¹⁵ Although these changes can be correlated to specific target binding with the nucleic acid recognition element, changes in charge-transfer resistance ($R_{\rm ct}$) and capacitance can also occur from nonspecific changes in the SAM¹⁵ or because of nonspecific adsorption events.¹⁶ It is thus important to take into consideration all possible modes of interfacial change through rigorous experimental controls.

The stability and reproducibility of the sensor interface are critical for the integrity of the analytical result to be surmised from the measurement (i.e., concentration, identity, etc.). To demonstrate this, Lazar et al.¹⁷ investigated the stability of electrochemically cleaned, bare gold electrodes under different electrolyte conditions, including phosphate buffer (PB) and $[Fe(CN)_6]^{3-/4-}$ (a typical redox couple used in EIS). They observed nonlinear, long-term drifts of R_{ct} , which they attributed to adsorption of electrolyte components on the surface and corrosion of the gold electrodes. 17 Vogt et al. 16 indicated that partial degradation of the $[Fe(CN)_6]^{3-/4-}$ redox mediator produces CN anions, which contribute to etching of the gold electrode surface. Using single-stranded (ss)DNAmodified electrodes, surface plasmon resonance (SPR) demonstrates a reversible increase and decrease in signal response after hybridization and dehybridization of a complementary strand, respectively. However, R_{ct} increased significantly after the first hybridization and dehybridization with a minor increase in R_{ct} after the second hybridization. The conflicting results between SPR and EIS indicated the possibility of CN⁻ etching the gold surface. Furthermore, Xu et al. 15 explored the stability and reproducibility of faradaic EIS analysis on mixed monolayers of aptamers and MCH. They observed changes in R_{ct} which were attributed to the reorganization of the monolayer to be thinner and more closely packed, especially for MCH monolayers. Moreover, Kelley et al. 18 observed dramatic changes in the monolayer thickness with applied potential for tethered DNA duplexes. They explained that tethered DNA duplexes may stand straight up or lie flat down on the metal surface at negative or positive potential, respectively.¹⁸ For surfaces modified with ssDNA, Jambrec et al. 19 proposed that switching the potential in high ionic strength buffers promotes the exchange of cations and anions between the electrode and the bulk solution, which creates a convection phenomenon. Negative potential repels the ssDNA to an upright position, whereas ssDNAs may bend down at positive potentials.¹⁹ In short, electrochemical methods of interrogating sensor surfaces affect the underlying sensing monolayer, and this does not take into account the thermodynamics of the nucleic acid structure of the electrode surface which also plays a role. 20,21

In this study, the nuanced effects of various solution conditions, nucleic acid probe geometries, and electrochemical sampling methods on the stability and performance of SAMs of aptamers with MCH formed on the gold sensing electrode are evaluated. In line with previous studies, we found that these factors matter, however not always in a linear fashion. To perform these studies, we employed various lengths and sequences (and thus structures) of ssDNAs co-immobilized with MCH with varying packing densities on polycrystalline gold electrode surfaces. The effects of the ssDNA length and varying sequences on the efficiency of probe immobilization were characterized. Furthermore, we demonstrate the effects of various $[\mathrm{Fe}(\mathrm{CN})_6]^{3-/4-}$ concentrations, cyclic voltammetry (CV), and EIS at various packing densities, taking into account several controls using no electrochemical treatment. We

investigate and discuss the EIS response in different electrolytes including PB saline (PBS) and PB and in the presence or absence of $[{\rm Fe(CN)_6}]^{3-/4-}$. EIS and surface coverage were recorded before and after repeated CV scans. Changes in $R_{\rm ct}$ and the different thermodynamics are explained for each ssDNA. The stability and performance of sensing surfaces are critical for the development of reproducible and sensitive sensors. Repeated electrochemical treatment in wide potential regimes can create defective ssDNA SAMs that may produce false or nonreproducible sensors.

EXPERIMENTAL SECTION

Materials and Chemicals. All chemicals and solvents used in this study were of analytical grade or better. The ultrapure deionized (DI) water purified with a Biopak Polisher (18.2 $M\Omega\cdot cm$, Millipore, Billerica, MA) had at least 18 $M\Omega$ resistivity.

PBS consisted of 10 mM sodium phosphate dibasic dihydrate (Na₂HPO₄·2H₂O), sodium phosphate monobasic dihydrate (NaH₂PO₄·2H₂O), sodium chloride (NaCl), and potassium chloride (KCl) from Sigma-Aldrich. Pure microcystin-LR and -RR as aptamer targets were obtained from Enzo Biochem, Inc. (Farmingdale, NY, USA). The four different lengths of ssDNAs (T7, T21, RR35, and LR60) with sequences are described in Table S1. The nucleic acids with and without methylene blue dye were synthesized by Integrated DNA Technologies (Coralville, IA, USA) and Biosearch Technologies (CA, USA). The ssDNA stocks were dissolved in Tris-EDTA, aliquoted, and stored at -24 °C. Methodology on the preparation of ssDNA monolayers is described in detail in the Supporting Information. Tris-2-carboxyethyl-phosphine, MCH, ruthenium(III) hexamine (RuHex), tris-base pH 7.4, and magnesium chloride solution (2 M in H₂O, MgCl₂) were purchased from Sigma-Aldrich. The single-stranded binding protein (SSBP) was obtained from Thermo Fisher Scientific Inc. Potassium ferricyanide (III) and potassium hexacyanoferrate (II) trihydrate were obtained from Sigma-Aldrich. All the chemicals were used without further purification.

Instrumentation and Electrochemical Measurements. All measurements were performed using a standard threeelectrode configuration with a 2 mm diameter gold working electrode, a platinum wire auxiliary electrode, and an Ag/AgCl (3 M NaCl) reference electrode (CH Instruments, Austin, TX). CV and chronocoulometric measurements were performed using a 1000C multipotentiostat (CH Instruments, Austin, TX). During CV interrogation, the potential scanning window was 0.8 to -0.150 V and the scan rate was 100 mV/s. Single-step chronocoulometry was conducted for initial surface coverage calculations using 50 μM RuHex. The potential step was from 0.1 to -0.4 V with a pulse width of 0.5 s, sample interval of 5 \times 10⁻⁴ s, and sensitivity of 1 \times 10⁻⁵ A/V. EIS measurements were conducted on an SP-150 Biologic instrument using a multi sine mode and a set potential of 0.226 V. Frequency ranged from 100 kHz to 100 mHz with a sinus amplitude of 5 mV. For all experiments, the modified Randles circuit (Figure S1) was used to fit the EIS data. Detailed procedures and methodologies are included in the Supporting Information.

Before electrochemical analyses, surface packing density was calculated and EIS data were collected, which served as the baseline. After each CV scan, surface coverage and charge-transfer resistance changes were calculated using the following equations

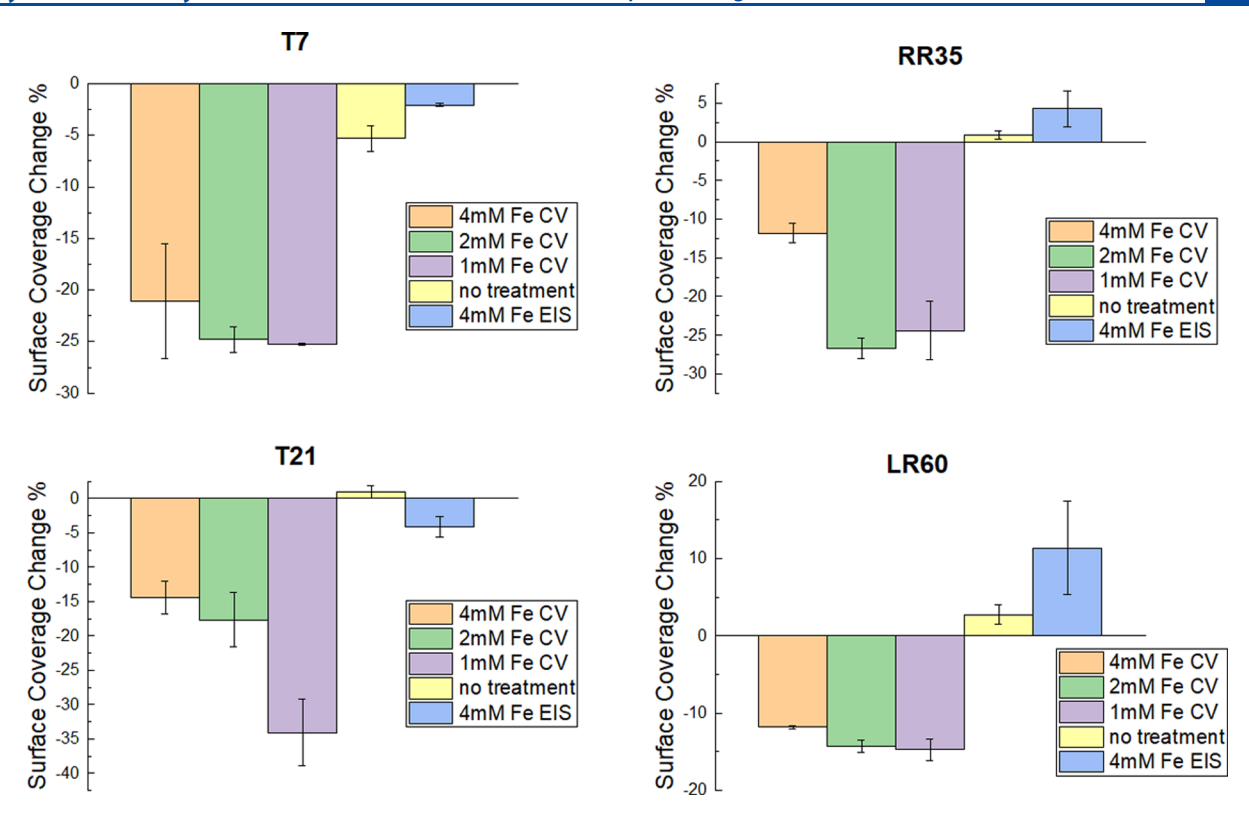


Figure 1. Electrochemical interrogation by CV and EIS, and solution conditions affect the surface coverage of DNA, as determined by CV using slow scan rates (redox molecule is methylene blue at the 3'end of aptamers). Columns illustrate the surface coverage difference before and after one CV cycle or EIS or no treatment for (top left) T7-, (bottom left) T21-, (top right) RR35-, and (bottom right) LR60-modified electrodes in 1, 2, and 4 mM Fe(CN) $_6^{3-/4-}$ in PBS. Fe represents the presence of Fe(CN) $_6^{3-/4-}$. All data points and error bars represent the mean and standard deviation of at least three independently modified electrode surfaces.

surface coverage change %

$$= (SC_{after} - SC_{before})/SC_{before} \times 100$$
 (1)

$$R - R_o = (R_{ct} \text{ after } - R_{ct} \text{ before})$$
 (2)

$$(R - R_o)/R_o$$
 % = $(R_{ct} \text{ after } - R_{ct} \text{ before})/R_{ct} \text{ before}$
× 100 (3)

where SC denotes surface coverage and R_{ct} is the recorded charge-transfer resistance before or after any treatment.

RESULTS AND DISCUSSION

A common electrode surface for EIS nucleic acid-based sensors is a mixed monolayer of 5' thiolated DNA and MCH. This surface serves as the basis for the studies reported herein with the addition of a 3'-methyene blue to serve as a redox reporter in voltammetric studies. Several key characteristics can be varied to affect the resulting sensor performance including the probe packing density and thus probe spacing, the nucleic acid probe sequence, and, consequently, the tertiary structure of the probe. We control packing density by controlling the DNA probe concentration utilized during SAM formation with a fixed time. Surface coverages are verified via both chronocoulometry and voltammetric methods (see Figure S2). The following results and accompanying discussion examine the effects of each parameter on the sensing surface stability to repeated electrochemical interrogations. Moreover, we also investigated the effects of several different solution conditions. All of the aforementioned parameters appear to affect the electrical responce of the sensing surface to electrochemical

interrogation. Packing densities presented in the following figures were determined via the CV method in Tris buffer using ssDNA-MB probes (raw data and details in the Supporting Information).

CV of [Fe(CN)₆]^{3-/4-} perturbs the sensing ssDNA monolayer significantly more so than EIS sweeps. In Figure 1, we show the immediate effects of CV and EIS scans on the SAM of ssDNAs T7, T21, RR35, and LR60 at packing densities of 10.91×10^{12} , 6.03×10^{12} , 4.16×10^{12} , and 2.77×10^{12} 10¹² molecules/cm², respectively. After scanning an EIS spectrum, we observed minimal effects on the packing density with a change in surface coverage of $+11.35 \pm 5.99\%$ to -2.04± 0.19% for all probes. A decrease in surface density is observed for polythymine chains, whereas a positive change is observed for the longer RR35 and LR60 aptamers. The negative change in surface coverage is expected if the thiolated aptamers desorb from the surface. Desorption of the thymine probe leads to a loss in the faradaic signal from the reduction of the 3'-attached methylene blue as the probe diffuses back into the bulk of the solution. Conversely, a positive change in surface coverage for random ssDNA sequences is presumably a result of the effects of DNA probe dynamics on the surface. More specifically, because measured current is a result of the redox mediator approaching the surface of the electrode, as larger probes are lost, the still-attached probes may have better access from reduced steric hindrance, and this, consequently, resulted in a higher measured current and thus calculated packing density.²² The calculated packing density is determined under the assumption that all 3'-methylene blue molecules reach the surface while performing slow scan rate

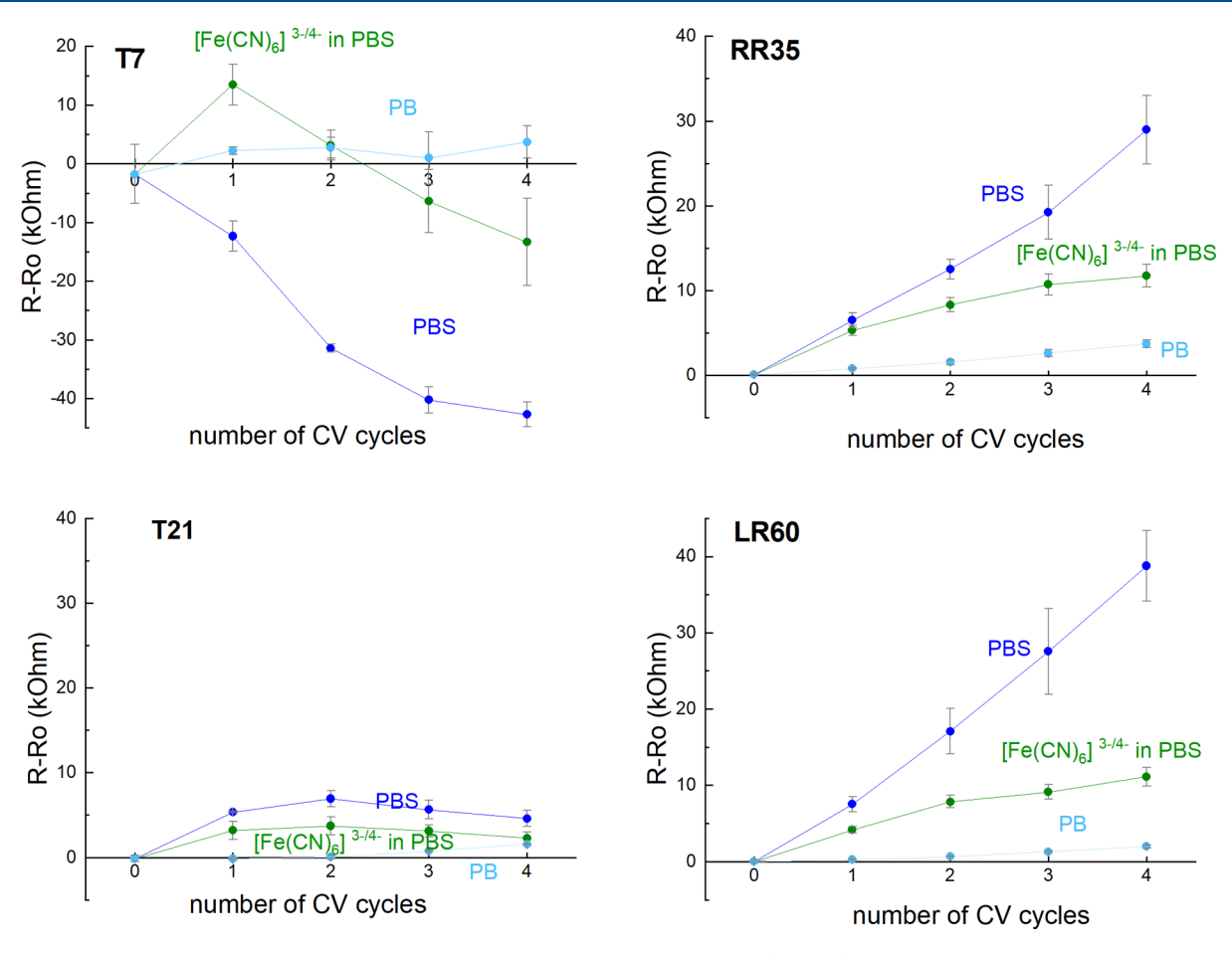


Figure 2. Effect of CV interrogation on charge-transfer resistance, as assessed by EIS $(R - R_o)$, on the electrode surface. The DNA-modified electrode surfaces were subjected to CV interrogation (0.8 to -0.15 V vs Ag/AgCl, $\nu = 100$ mV/s) in different electrolyte solutions (PBS buffer, PB buffer) with and without 4 mM $[Fe(CN)_6]^{3^{-/4}}$. All surfaces modified with (top left) T7, (bottom left) T21, (top right) RR35, and (bottom right) LR60 show changes, with the minimal perturbation observed for surfaces with the T21 probe. Charge-transfer resistance was calculated using the Randles circuit after EIS measurements. All data points and error bars represent the mean and standard deviation of at least three independently modified electrode surfaces. The lines are to guide the reader's eye.

experiments; however, this may not always be true. Consequently, when steric hindrance is reduced, the number of methylene blues that are able to reach and exchange electrons with the electrode outnumbers the number of probes lost during the electrochemical interrogations. Moreover, we attribute this odd result to aptamer conformational changes and possible rearrangement of the ssDNA and MCH monolayer. The two- and three-dimensional structures of the aptamer probes may be altered during EIS, either because of desorption of a number of probes or because of disruption of the aptamer monolayer and subsequent rearrangement of the monolayer.

Altering the potential using a CV scan in the presence of ferricyanide solution resulted in a decrease in surface coverage from $-11.8\pm1.21\%$ to $-34.1\pm4.85\%$. We attribute the probe desorption to the electrostatic repulsion of the negatively charged backbone of the nucleic acids from the surface, which decreases the binding energy of the molecules on the surface. Using various concentrations of Fe-(CN) $_6^{3-/4-}$, we observed a significant decrease in packing density when a lower concentration of Fe(CN) $_6^{3-/4-}$ (1 mM) was present in bulk solution. With increasing concentration of ferricyanide, its reduction may be favored over other reactions. This may also depend on the different two- and three-dimensional structures of DNA probes; however, it is not fully

understood. Finally, control experiments (without electrochemical treatment, using electrodes dipped in 4 mM ${\rm Fe(CN)_6}^{3-/4-}$ for an hour) had a minimum impact on the monolayer.

The choice of the electrolyte for electrochemical analysis is critical for achieving a controlled sensing surface with a correlative stable signal response for EIS. In an attempt to validate the decrease in packing density, we evaluated changes in R_{ct} in between measurements using EIS (Figure 2). Changes in the electrical double layer caused by adsorption or desorption of molecules on the electrode surface lead to an increase or decrease in the $R_{\rm ct}$ and capacitance values. To evaluate these events, we investigated three different electrolyte compositions (Table S2). In order to determine the effect of different compounds on the ssDNA monolayer, we gradually excluded compounds and observed the relative drop or rise in resistance. Impedance measurements in the presence of different electrolytes were explored with respect to the change in the charge-transfer resistance $(R - R_0)$ before and after the application of four CV cycles. Control experiments include the recorded $R - R_o$ when only EIS measurements were applied (Figures 2 and 3A as "0 CV cycles"). The four different lengths of nucleic acids were evaluated using electrodes with the highest packing density acquired during chronocoulometric experiments. Anticipated results of this investigation would be

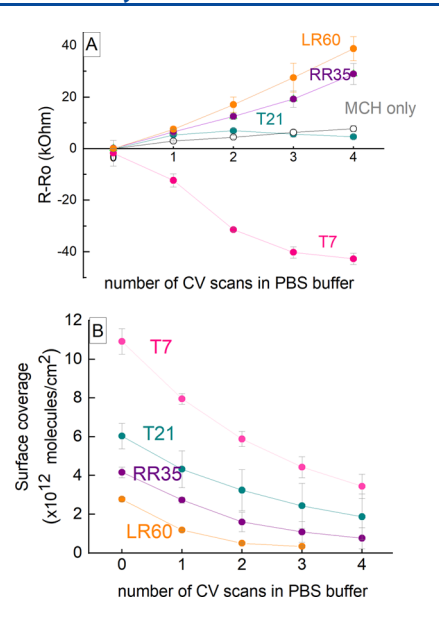


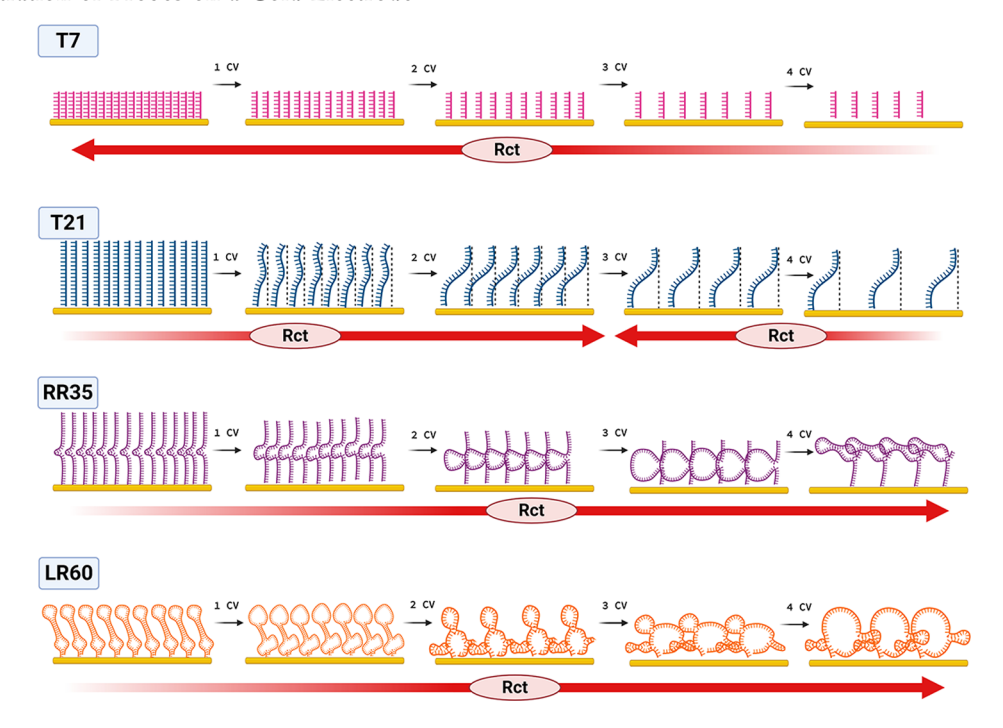
Figure 3. Effect of continued voltammetric interrogation of DNA-modified electrodes on surface coverage for all lengths of ssDNA tested (T7, T21, RR35, and LR60). The graphs illustrate the difference in (A) charge-transfer resistance and (B) surface coverage as a function of the number of CV scans in PBS buffer. All aptamers were modified with methylene blue at the 3'-end. All data points and error bars represent the mean and standard deviation of at least three independently modified electrode surfaces. For LR60, surface coverage for the fourth CV cycle could not be determined because of the low sensitivity of the method. The lines are to guide the reader's eye.

that phenomena related to specific or nonspecific adsorption of molecules from the bulk lead to higher resistance, whereas in desorption, it would lower resistance. However, our results showed that this interpretation might not always be correct. CV interrogation of the ssDNA-modified gold electrode surface influenced $R_{\rm ct}$ leading to an observed increase in $R_{\rm ct}$ for most cases (except for surfaces prepared with T7 and partially with T21). Overall, in the presence of ${\rm Fe(CN)_6}^{3-/4-}$, the effect on $R-R_{\rm o}$ was not as significant as in its absence. Furthermore, experiments in pristine PB without saline showed only a small drift in $R_{\rm ct}$. Decreasing ionic strength causes the persistence length of the DNA to increase, decreasing the end-to-surface collision rate of the surface-bound ssDNA. In this regard, the ssDNA strands in the monolayer are not significantly affected by the electric field. These observations draw our attention to the relative influence on the monolayer and the surface of the electrode in higher ionic strength solutions, such as PBS buffer.

Changes in signal response depend on changes in packing density, which are interdependent with the relevant thermodynamic and structural properties of the tethered ssDNA at a given packing density. We grouped the data for all lengths of nucleic acids using PBS buffer as the electrolyte in Figure 3A and recorded packing density after each CV (Figure 3B). The EIS signal response for short polythymine-tethered ssDNA probes diverge in trend and magnitude from long random multibase probes of ssDNA. The structural changes that they might undergo are depicted in Scheme 1 and explained separately for each ssDNA in the following paragraphs.

Dense polythymine (T7) monolayers $(10.91 \times 10^{12} \text{ molecules/cm}^2)$ exhibited a decrease in EIS response with decreased packing density. Polythymine has a low propensity to form intrastrand stacked conformations;²⁵ therefore, polythymine chains are more likely to stand as rigid rods at high packing densities.²⁶ This is especially true for short T7 probes because the persistence length of short ssDNA $(0.8-1.3 \text{ nm}^{27})$ is comparable to the length of the probes (length of

Scheme 1. Illustration of Probes on a Gold Electrode^a



[&]quot;Decreasing surface coverage and structural changes over multiple CV scans in PBS buffer for T7, T21, RR35, and LR60. The illustrations of RR35 and LR60 correspond to secondary structures predicted using mfold software (see the Supporting Information). Created with BioRender.com.

T7 = 2.4 nm). ²⁸ Also, rigid rodlike structures are expected when probe-to-probe separation (interprobe distance, nm) is small and, certainly, in dense monolayers where T7 probe-to-probe separation approaches the value of 1.9 nm. With the loss of tethered probes, defects on the gold surface allow a faster electron transfer, which decreases $R_{\rm ct}$ (Scheme 1).

The polythymine probe T21 exhibited decreasing surface coverage along with a fluctuating R_{ct} . For the first two CV cycles, R_{ct} increased; however, after the second CV cycle, R -Ro decreased in value. This phenomenon is attributed to thermal fluctuations. More specifically, electrostatic interactions and dispersion interactions between the individual polythymine probes contribute to entropic elasticity.²⁹ Polythymine chains display purely entropic elasticity that may affect the conformational dynamics, depending on the packing density. At high surface coverage, enthalpic energy cannot overcome the structural transition and probes stand as rigid rods that may lean on each other (Scheme 1). However, at lower packing densities, low interactions and neglegible elasticity may contribute to a coil-helix transition.²⁶ after the first two CV cycles (a loosely packed density), bentdown DNA strands or coil-helix-shaped strands may cause a physical blocking of access to the electrode surface³⁰ and each strand occupies its projected area (Scheme 1).³¹ Any defects in the monolayer or gaps between the probes may influence the EIS signal significantly via the creation of pathways to the electrode surface for $Fe(CN)_6^{3-/4-15}$ The redox molecules approach the surface of the electrode through these pathways and finally enable the electron transfer. However, if the projected area of a bent-down probe blocks the surface of the electrode, then reduction of Fe3+ during EIS occurs at a slower rate, resulting in higher resistance. Also, other investigators reported that long polythymine chains result in disordered polyelectrolyte brushes.²⁸ Disordered polythymine arrays of probes of 21 or longer may disable the flow of current across the interface leading to an increased R_{ct} .

Longer random ssDNA sequences (RR35 and LR60) respond similarly to CV scans with a considerable increase in R_{ct}. The SAMs for these ssDNA were lower in density (than T7 and T21) and hence more susceptible to the impact of the electric field.³⁰ We observed an increasing trend in resistance with decreasing surface coverage. This is attributed to conformational changes and transition of different 2D structures (Scheme 1). In higher packing densities, the ssDNA probes of RR35 are forced into narrow alignment and adjust to a conformation of upward orientation.³⁰ After desorption of probes, even though fewer aptamer probes are attached on the gold surface, the transition to a different structure blocks the surface of the electrode, which finally leads to increased R_{ct}. Longer nucleic acid corresponds to a higher R_{ct} after each CV scan. This is probably due to structurally bulkier molecules that require more space on the surface of the gold electrode (Scheme 1). This is especially true for LR60 where the probe-to-probe separation is remarkably larger after four CV scans (see the Supporting Information). Other investigators supported the idea of possible flattened configurations and the presence of multiple adsorption contacts between the ssDNA and the gold surface.³² electrostatic adsorption of the negatively charged DNA onto the positively charged surface of the gold electrode might be another reason.³³ Moreover, strongly ionized polymer brushes may produce the "osmotic" regime where the majority of the mobile counter ions are trapped within the highly charged

brush monolayer to compensate the immobilized negatively charged backbone of ssDNA.³⁴ Under an applied electric field during voltammetry, more counterions may be forced to entrap in between the brushes. These ions might be hydrated Cl⁻, Na⁺, and K⁺ or even polarized water molecules. Furthermore, a previous report on the stability of SAMs of nucleic acids has shown similar drift in EIS.¹⁵ A possible cause of this drift was attributed to reorganization of the monolayer into a thinner monolayer, but with closely relocated tethered MCH molecules.¹⁵

Desorption efficiency increases proportionally to the ssDNA length. In Figure 3B, all ssDNAs followed a similar desorption trend; however, the desorption efficiency [(SC_{after} – SC_{before})/SC_{before} × 100] was different for each ssDNA. Observed desorption efficiencies of 49.0% for LR60, 34.5% for RR35, 25.4% for T21, and 25.0% for T7 showed that in the case of long and multibase probes, the impact of CV treatment is greater than that in short and monobase thymine probes. Also, this substantiates again that a lower surface coverage is more vulnerable to the electric field than higher packing densities.

Controls of MCH monolayers on electrodes showed a drift in EIS as well. The degree of the drift is comparable to that of T21, but relatively smaller when compared to RR35 and LR60 (Figure 3A). Recent studies associate the increased R_{ct} with a reorganization of a thinner and more compact MCH layer. 1 The underlying thermodynamic changes are more complex. Densely tethered molecules may entrap counter ions to balance out the charge. However, in high-potential regimes (0.8 to -0.150 V in our study), hydrated sodium ions may adhere on top of the MCH monolayer.³³ A possible scenario could be that the electric field may be damaging and splitting the hydroxyl groups or hydrogen atoms, leaving behind tethered MCH molecules with dangling bonds at the alkane chain. These dangling bonds may serve as binding sites for the thiol groups of MCH molecules that are captured during rearrangement of the monolayer and create a stacked chain of MCH molecules.³⁵ Even though all these are important considerations, the effects of CV on an electrolyte, such as PBS, and on an MCH-modified monolayer are not yet fully understood.

We further attempted to verify the desorption of ssDNA probes from the surface of the electrode by examining the EIS response upon binding of a biomolecular target. In this regard, we used SSBP, a protein with 177 amino acids and a molecular weight of 18,873 g/mol.³⁶ In general, SSBPs have the ability to bind to ssDNA and protect the ssDNA from nucleases until it can be replicated.³⁷ We tested the binding effect of SSBP on all four ssDNAs before and after the application of CV cycles (Figure 4A). For highly packed and short T7 probes, binding of SSBP was relatively low in both CV-unaffected and CVaffected electrodes. Other investigators observed a significant decrease in SSBP affinity when the length of ssDNA is reduced to 7 bases.³⁸ Also, for electrodes with high surface coverage, binding is expected to decline, especially when big targets such as SSBP are used.²⁸ Furthermore, T21 had the highest signal change in resistance of all tested probes. With increasing length of ssDNAs (RR35 and LR60), we observed a decreasing signal change in percentage for $R_{\rm ct}$ [$(R - R_{\rm o})/R_{\rm o}$ %]. CV-unaffected electrodes had considerably higher $(R - R_o)/R_o$ % than the CV-affected ones. This implies that less ssDNA is on the surface of the electrode after CV application. To appraise this conclusion, we also tested the binding of SSBP over several probe packing densities, specifically for T21, which was chosen

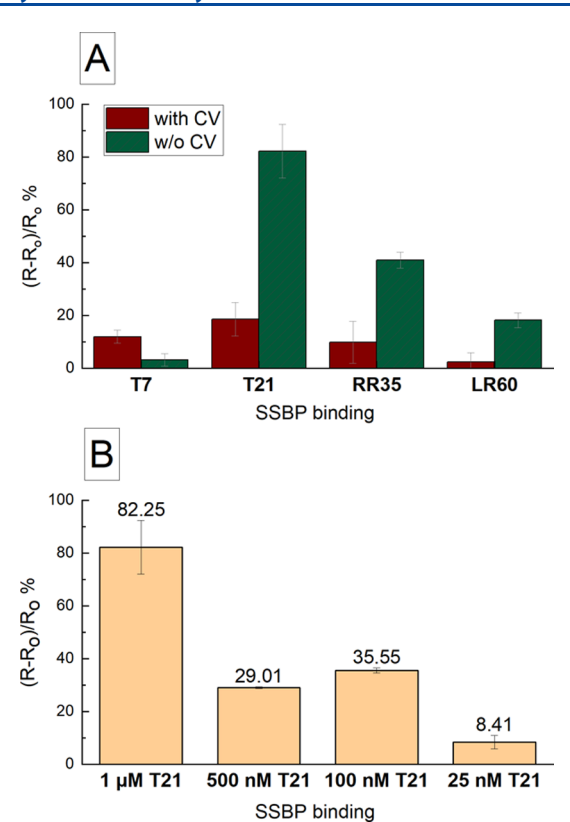


Figure 4. (A) Signal change in charge-transfer resistance after incubation with 50 μ g/mL SSBP for four ssDNAs with different lengths: T7, T21, RR35, and LR60. Comparison between the initial unaffected (green bars) modified electrodes and after CV in PBS buffer (brown bars). All data points and error bars represent the mean and standard deviation of at least three independently modified electrode surfaces. (B) Signal change in charge-transfer resistance after incubation with 50 μ g/mL SSBP for different packing densities of T21.

because of its high signal change of 82.3% for unaffected electrodes. For electrodes prepared with T21 concentration ranging from 1 μ M to 25 nM, $(R-R_{\rm o})/R_{\rm o}$ % appeared to decrease proportionally to packing density (Figure 4B). Nevertheless, the desorption of nucleic acids, transition to a different two-dimensional structure, or nonspecific adsorption contributed to a diminished performance of the sensing surfaces in the binding event of SSBP.

CONCLUSIONS

In this paper, we demonstrate and describe the nuanced effects of various nucleic acid-based sensors parameters (nucleic acid length, structure, and packing density) and interrogation methods (electrochemical technique, buffer composition, and redox mediators) on the stability of the sensing monolayer and consequent effects on signaling fidelity. We found that the signal can vary in both positive and negative gains in $R_{\rm ct}$ which, if left unchecked, can lead to false positives during sensing experiments (example in the Supporting Information). For example, under certain conditions, CV scanning disturbs ssDNA monolayers extensively, whereas EIS has minimal effects on the surface density. We hypothesized that changes in signal after electrochemical interrogation are likely due to the loss of thiolated nucleic acid probes from the surface of the electrode. Desorption of probes provides the remaining DNA probes with greater spacing between them which could

potentially alter the two- and three-dimensional structures of the ssDNA probes, further exacerbating the current and the R_{ct} signal change in both positive and negative directions. The relative change in signal response is dictated by the secondary structure of the probe and whether or not the rearranged DNA blocks the surface of the electrode. Bulkier structures will disable electron transfer, which results in a higher R_{ct} , whereas structures with a smaller footprint will allow electron transfer that leads to a lower R_{ct}. Finally, SSBP binding affinity was found to be lower for electrochemically treated electrodes than untreated electrodes, verifying that charged sensing interfaces were losing DNAs causing performance to decrease. EIS is an effective technique to use when all thermodynamics and geometries of the system have been considered. Experimental planning that avoids repetitive application of potentials is necessary to ensure reliable EIS measurements. Controlled electrolyte conditions are also crucial to experiment using stable and reliable monolayers and acquire meaningful data to interpret. Last but not the least, structured experiments including controls are absolutely necessary when using ssDNA-modified sensing surfaces.

In short, a comprehensive characterization of the sensor system under development is essential for improving the performance and veracity of an analytical method. Considering the extensive use of nucleic acid monolayers as sensing surfaces for the detection of important biomarkers or environmental contaminants and the use of EIS as a signal transduction method, $R_{\rm ct}$ fluctuations due to structural changes or nonspecific adsorption critically affect the performance of such surfaces. Reproducible sensing surfaces that perform in complex environments can be reliable only after adequate experimental work with controls has been conducted. This work shows the importance of controls to prevent false positives in detection of targets. Moreover, this study provides guidance to produce relatively stable monolayers for electrochemical sensing applications.

ASSOCIATED CONTENT

Supporting Information

The Supporting Information is available free of charge at https://pubs.acs.org/doi/10.1021/acs.analchem.0c03269.

Details on predicted 2D structures, samples of CV and EIS raw data, surface coverage, probe-to-probe estimated values, and example of false positives (PDF)

AUTHOR INFORMATION

Corresponding Authors

Ryan J. White — Department of Chemistry and Department of Electrical Engineering and Computer Science, University of Cincinnati, Cincinnati, Ohio 45221-0172, United States; orcid.org/0000-0003-0849-0457; Email: white2r2@ucmail.uc.edu

Dionysios D. Dionysiou — Environmental Engineering and Science Program, Department of Chemical and Environmental Engineering (ChEE), University of Cincinnati, Cincinnati, Ohio 45221-0012, United States; orcid.org/0000-0002-6974-9197; Email: dionysdd@ucmail.uc.edu

Authors

Vasileia Vogiazi – Environmental Engineering and Science Program, Department of Chemical and Environmental

Engineering (ChEE), University of Cincinnati, Cincinnati, Ohio 45221-0012, United States

Armah de la Cruz – Office of Research and Development, US Environmental Protection Agency, Cincinnati, Ohio 45268-0001, United States

William R. Heineman — Department of Chemistry, University of Cincinnati, Cincinnati, Ohio 45221-0172, United States; orcid.org/0000-0003-2428-5445

Complete contact information is available at: https://pubs.acs.org/10.1021/acs.analchem.0c03269

Notes

The authors declare no competing financial interest.

ACKNOWLEDGMENTS

The authors would like to thank Dr. Yao Wu and Dr. Robert Lazenby for helpful discussions. This work was supported by the National Science Foundation, Division of Chemical, Bioengineering, Environmental & Transport Systems, with award no. 1706489.

REFERENCES

- (1) Vogiazi, V.; De La Cruz, A.; Mishra, S.; Shanov, V.; Heineman, W. R.; Dionysiou, D. D. ACS Sens. **2019**, *4*, 1151–1173.
- (2) Villalonga, A.; Pérez-Calabuig, A. M.; Villalonga, R. Anal. Bioanal. Chem. 2020, 412, 55–72.
- (3) Brothers, M. C.; Moore, D.; Lawrence, M. S.; Harris, J.; Joseph, R. M.; Ratcliff, E.; Ruiz, O. N.; Glavin, N.; Kim, S. S. Sensors 2020, 20, 2246.
- (4) Oberhaus, F. V.; Frense, D.; Beckmann, D. Biosensors 2020, 10, 45.
- (5) West, R. M. J. Electrochem. Soc. 2020, 167, 037544.
- (6) Wu, Y.; Midinov, B.; White, R. J. ACS Sens. 2019, 4, 498-503.
- (7) Macazo, F. C.; Karpel, R. L.; White, R. J. Langmuir 2015, 31, 868-875.
- (8) Santos-Cancel, M.; Simpson, L. W.; Leach, J. B.; White, R. J. ACS Chem. Neurosci. 2019, 10, 2070–2079.
- (9) Acquah, C.; Danquah, M. K.; Yon, J. L. S.; Sidhu, A.; Ongkudon, C. M. Anal. Chim. Acta 2015, 888, 10–18.
- (10) Adachi, T.; Nakamura, Y. Molecules 2019, 24, 4229.
- (11) Zhang, Y.; Lai, B.; Juhas, M. Molecules 2019, 24, 941.
- (12) Sun, C.; Liu, M.; Sun, H.; Lu, H.; Zhao, G. Biosens. Bioelectron. 2019, 140, 111352.
- (13) Ravalli, A.; Voccia, D.; Palchetti, I.; Marrazza, G. Biosensors 2016, 6, 39.
- (14) Afsarimanesh, N.; Mukhopadhyay, S. C.; Kruger, M. Planar Interdigital Sensors and Electrochemical Impedance Spectroscopy. *Smart Sensors, Measurement and Instrumentation*; Springer International Publishing, 2019; Vol. 30, pp 33–44.
- (15) Xu, X.; Makaraviciute, A.; Kumar, S.; Wen, C.; Sjödin, M.; Abdurakhmanov, E.; Danielson, U. H.; Nyholm, L.; Zhang, Z. *Anal. Chem.* **2019**, *91*, 14697–14704.
- (16) Vogt, S.; Su, Q.; Gutiérrez-Sánchez, C.; Nöll, G. Anal. Chem. 2016, 88, 4383-4390.
- (17) Lazar, J.; Schnelting, C.; Slavcheva, E.; Schnakenberg, U. Anal. Chem. 2016, 88, 682–687.
- (18) Kelley, S. O.; Barton, J. K.; Jackson, N. M.; McPherson, L. D.; Potter, A. B.; Spain, E. M.; Allen, M. J.; Hill, M. G. *Langmuir* **1998**, *14*, *6781*–*6784*.
- (19) Jambrec, D.; Gebala, M.; La Mantia, F.; Schuhmann, W. Angew. Chem., Int. Ed. 2015, 54, 15064–15068.
- (20) Lipfert, J.; Doniach, S.; Das, R.; Herschlag, D. Annu. Rev. Biochem. 2014, 83, 813-841.
- (21) Vainrub, A.; Pettitt, B. M. Chem. Phys. Lett. 2000, 323, 160–166.

- (22) Huang, K.-C.; White, R. J. J. Am. Chem. Soc. 2013, 135, 12808–12817.
- (23) Arinaga, K.; Rant, U.; Knežević, J.; Pringsheim, E.; Tornow, M.; Fujita, S.; Abstreiter, G.; Yokoyama, N. *Biosens. Bioelectron.* **2007**, 23, 326–331.
- (24) Huang, K.-C.; White, R. J. J. Am. Chem. Soc. 2013, 135, 12808–12817.
- (25) Chakraborty, K.; Khatua, P.; Bandyopadhyay, S. Phys. Chem. Chem. Phys. 2016, 18, 15899-15910.
- (26) Mishra, G.; Giri, D.; Kumar, S. Phys. Rev. E: Stat., Nonlinear, Soft Matter Phys. 2009, 79, 1539-3755.
- (27) Tinland, B.; Pluen, A.; Sturm, J.; Weill, G. Macromolecules 1997, 30, 5763-5765.
- (28) Halperin, A.; Buhot, A.; Zhulina, E. B. *Biophys. J.* **2005**, 89, 796–811.
- (29) Goddard, N. L.; Bonnet, G.; Krichevsky, O.; Libchaber, A. *Phys. Rev. Lett.* **2000**, *85*, 2400–2403.
- (30) Gębala, M.; Schuhmann, W. ChemPhysChem **2010**, 11, 2887–
- (31) Ho, J.-J.; Skoff, D. R.; Ghosh, A.; Zanni, M. T. J. Phys. Chem. B **2015**, 119, 10586–10596.
- (32) Levicky, R.; Herne, T. M.; Tarlov, M. J.; Satija, S. K. J. Am. Chem. Soc. 1998, 120, 9787–9792.
- (33) Watkins, H. M.; Ricci, F.; Plaxco, K. W. Langmuir 2018, 34, 14993-14999.
- (34) Rao, A. N.; Grainger, D. W. Biomater. Sci. 2014, 2, 436-471.
- (35) Kummer, K.; Vyalikh, D. V.; Gavrila, G.; Kade, A.; Weigel-Jech, M.; Mertig, M.; Molodtsov, S. L. J. Electron Spectrosc. Relat. Phenom. **2008**, 163, 59–64.
- (36) Sancar, A.; Williams, K. R.; Chase, J. W.; Rupp, W. D. Proc. Natl. Acad. Sci. U.S.A. 1981, 78, 4274–4278.
- (37) Spiering, M. M.; Benkovic, S. J. DNA Replication Fork, Bacterial. *Encyclopedia of Biological Chemistry*, 2nd ed.; Elsevier Inc., 2013; pp 114–117.
- (38) Kunzelmann, S.; Morris, C.; Chavda, A. P.; Eccleston, J. F.; Webb, M. R. *Biochemistry* **2010**, *49*, 843–852.